From superresolution to nanodetection: overview of far field optical nanoscopy techniques for nanostructures

P C Montgomery[1], A Leong-Hoi[1], F Anstotz[1], D Mitev[2], L Pramatarova[2] and O Haeberlé[3]

[1]Laboratoire des Sciences de l'Ingénieur, de l'Informatique et de l'Imagerie (ICube), University of Strasbourg-CNRS,23 rue du Loess, 67037 Strasbourg, France
[2]Georgi Nadjakov Institute of Solid State Physics, Bulgarian Academy of Sciences, 72 Tzarigradsko Chaussee blvd., 1784 Sofia, Bulgaria
[3] Laboratoire MIPS, Universite de Haute-Alsace, Ecole Nationale Supérieure d'Ingénieurs Sud Alsace (ENSISA), 12 rue des Frères Lumière, 68093 Mulhouse, France

E-mail : paul.montgomery@unistra.fr

Abstract. Far field optical nanoscopy has been brought to the forefront with the 2014 Nobel Prize for chemistry in fluorescent nanoscopy for revealing intra-cellular details of tens of nm. In this review, we present an improved classification scheme that summarizes the many optical nanoscopy techniques that exist. We place particular emphasis on unlabelledsuperresolution techniques that provide real improved resolving power and unlabellednanodetection techniques for characterizing unresolved nanostructures. Superresolution is illustrated with sub-100 nm imaging of diatoms with tomographic diffractive microscopyand adenoviruseswith submerged microsphere optical nanoscopy. Three sub-categories of nanodetectionare then presented. Contrast enhancement is illustrated with surface enhanced ellipsometric contrast microscopy for the study of bacterial motility and strobed phase contrast microscopy for measuring the mechanical properties of vesicle membranes. High sensitivity phase measurement using interference microscopy demonstrates how nanostructured surfaces and structures can be characterized in biomaterials, laser textured stainless steel and defects within thin polymer films. Finally, deconvolution is illustrated with the use of through-focus scanning optical microscopy in critical dimension measurement and characterization of 40 nm linewidths in microelectronic devices. In this way we show how new far field optical nanoscopy techniques are being developed for unlabelled characterization of nano and biomaterials.

1. Introduction

To help in the understanding and development of nano and biostructures, new imaging techniques are required that are capable of sub-cellular resolution and nanodetection over wide fields. The use of light in far field optical nanoscopy has been brought to the forefront with the 2014 Nobel Prize for chemistry [1], with fluorescent stimulated emission depletion microscopy (STED) [2] achieving a real optical lateral resolution of 30 nm and single molecule microscopy [3, 4] capable of revealing intra-cellular details of tens of nm using the superlocalization of fluorescent marker molecules. Several far field nanoscopy techniques and principles without using labelling had already been developed in materials science at the beginning of the 1990's [5, 6] and in [7] we presented a first classification scheme of the main optical nanoscopy techniques in order to help to better understand their different

approaches and performances that we improved in [8]. In the present review, we further extend the classification scheme (figure 1) with additional techniquesand categories which differentiatethe unlabelled techniques(grey area) from those requiring the use of fluorescent or gold nanomarkers.

As highlighted in the work of S. Hell with STED [9], overcoming the classical resolution limit due to diffraction in fluorescence microscopy came from the realization that resolution was limited by the principle of controllable on/off states in fluorescence molecules, followed by contrast limits and superlocalization. Structured illumination microscopy (SIM) [10] also allows superresolution.

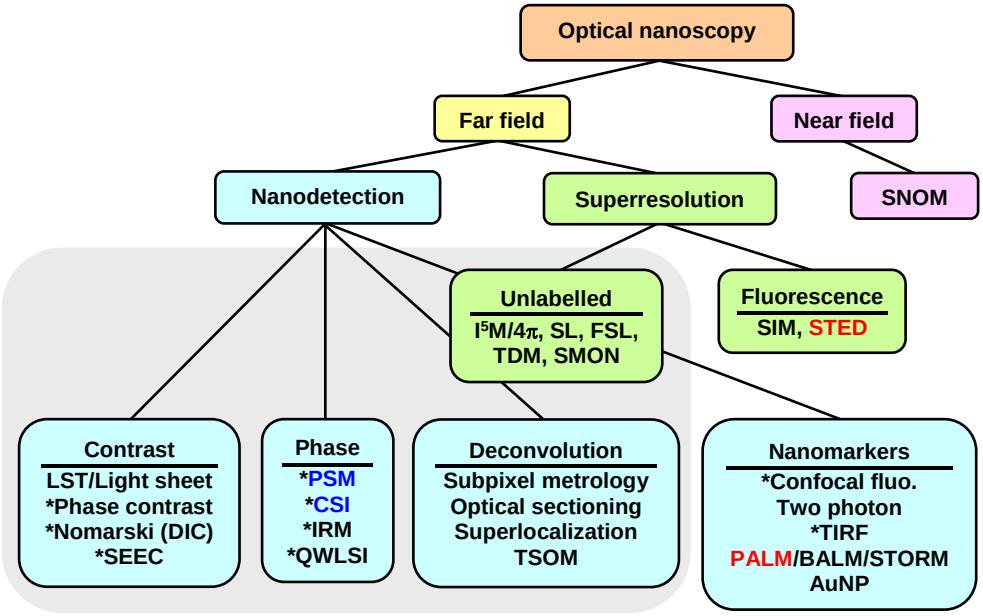

Figure 1. Improved classification scheme of optical nanoscopy techniques.
Notes: *indicates the possibility of real time imaging, red words show the two techniques honored by the 2014 Nobel Prize for chemistry, blue words show techniques being developed further at ICube and the grey area shows unlabelled far field nanoscopy techniques.

Abbreviations: 4π, 4π microscopy; AuNP, gold nanoparticles; BALM, bleaching (or blinking) assisted localization microscopy; Confocal fluo, confocal fluorescence microscopy; CSI, coherence scanning interferometry; FSL, far field superlens; I^5M, combination of I^2M (interference illumination microscopy) and I^3M (incoherent interference illumination microscopy); IRM, interference reflection microscopy; LST, laser scanning tomography; Nomarski, differential interference contrast (DIC) microscopy; PALM, photo-activated localization microscopy; PSM, phase-stepping microscopy; QWLSI, quadriwave lateral shearing interferometry; SEEC, surface enhanced ellipsometric contrast microscopy; SIM, structured illumination microscopy; SL, scattering lens microscopy; SMON, submerged microsphere optical nanoscopy; SNOM, scanning near-field optical microscopy; STED, stimulated emission depletion; STORM, stochastic optical reconstruction microscopy; TDM, tomographic diffractive microscopy; TIRF, total internal reflection; TSOM, through-focus scanning optical microscopy.

An important distinction is made between superresolution techniques that provide real improved resolving power compared with the classical λ/2 limit of diffraction and nanodetection techniques that are used to characterize unresolved nanostructures [11]. Concerning the category ofsuperresolution techniques, we illustrate first among the unlabelled approaches results from tomographic diffractive microscopy (TDM), giving a resolution of 97 nm in the imaging of diatoms [12]. A second technique is described by submerged microsphere optical nanoscopy (SMON) [13] that uses the unusual properties of photonic nano-jets [14] to observe adenoviruses that are less than 100 nm in size.

The second category concerns nanodetection techniques and is divided into four sub-categories that make use of the contrast, phase, deconvolution or nanomarkers to achieve nanodetection. Unlabelled contrast enhancement is illustrated with surface enhanced ellipsometric contrast microscopy (SEEC) [15], using polarized light and a dedicated thin film coated substrate to reveal nano-thin slime trails of bacteria for studying their motility. A second contrast enhancing technique is also presented, real time phase contrast microscopy to reveal the vibration modes of the 5 nm thick lipid walls of giant vesicles [16]. Very high sensitivity phase measurement is demonstrated by our own results using improved modes of coherence scanning interferometry (CSI, marked in blue in figure 1) of the study of biomaterial nanostructures [17, 18], nanotextured stainless steel surfaces [19] and μm defects in thin Mylar polymer films[20] by means of carefully controlled image processing. Finally, a technique using deconvolution, through-focus scanning optical microscopy (TSOM)[21], is presented to demonstrate how nanostructures on semiconductor surfaces can be measured to within nm. The well-controlled use of the optical response of ordinary optical microscopes demonstrates not only the measurement of 40 nm linewidths in microelectronic devices to within 1 nm, but the availability of a wealth of other useful information such as sidewall angle and the detection of nanoparticles and the distinction between different numbers of clumps of nanoparticles.Nanodetection techniques using nanomarkers [1, 3, 4] such as photo-activated localization microscopy PALM, bleaching (or blinking) assisted localization microscopy (BALM) and stochastic optical reconstruction microscopy STORM are not described here, having been covered in [7, 9]. In this review, we highlight in particular nanoscopy techniques that are capable of superresolution or nanodetection and do not require labelling of the sample but nonetheless reveal details or information about nanostructures.

2. Unlabelled superresolution nanoscopy

The lateral resolution in standard optical microscopy is generally accepted to be limited by the effects of diffraction, given by the Rayleigh criterion, $R_l = 0.61\times\lambda/NA$, where λ is the wavelength of the light from the sample, and NA is the numerical aperture of the imaging lens, given by $NA = n\times\sin\alpha$, where n is the refractive index of the imaging medium and α is the half-angle of the light cone that can enter the objective. Using visible light and a high NA objective in air, this gives a typical resolution limit of about 0.4 μm and 0.2 μm with an oil immersion lens in blue light [22]. This value can be improved further by up to 30% in confocal microscopy by means of an optimized imaging system consisting of point illumination and a pinhole in front of the detector to eliminate out-of-focus signals. Further selectivity is achieved with total internal reflection microscopy (TIRF) [23] and two photon microscopy [24].

In recent decades, several superresolution techniques have been developed that give a real increase in resolving power of the imaging system, so leading to the observation of finer details, the most successful being in fluorescence microscopy. Well known techniques are STED microscopy [2, 9], and SIM microscopy [10].While fluorescence microscopy techniques lead to the advantages of improved resolution and the targeting of specific proteins in living cells, they are dependent on the use of labelling with fluorescent molecules which is intrusive and limits the time of light exposure to tens of seconds due to photobleaching. Unlabelled nanoscopy techniques have the advantages of being less intrusive and open to a wider number of objects that can be imaged. Several new techniques that do not require labelling exist, amongst themI^5M, 4πillumination [25],SL microscopy [26, 27] and FSL microscopy[28]. In this section we highlight just two new techniques, namely TDM and SMON.

2.1. Tomographic diffractive microscopy (TDM)

Much of the information concerning the shape of a microscopic sample, such as its surface and 3D structure can be saved in a digital hologram using the technique of digital holographic microscopy (DHM). However, reconstructed images from digital holograms generally have low lateral resolution due to limited spatial frequencies in the Fourier domain which is degraded further by speckle noise.

In TDM, the tomographic mode of DHM, one solution to improve the resolution is to vary the illumination angle so as to increase the synthetic aperture size and increase the spatial frequencies

available [12].In addition, the use of many different illumination angles averages the speckle noise, improving further the details observable. Using phase shifting interferometry, the incident wave diffracted by the specimen is measured in the Fourier domain at different illumination angles. A three-dimensional representation of the object is then reconstructed using the series of images recorded at each angle in the spatial frequency domain. By means of the first approximation of Born [22] and a simple Fourier transform, the distribution of the complex refractive index within the sample is then obtained.TDM thus allows high resolution imaging of transparent unlabelled specimens, up to twice the resolution possible in classical microholography, or λ/(4×NA) in the transmission mode.

An example of some results using TDM is shown in figure 2, consisting of a series of reconstructed images viewed from 6 different angles of a diatom which is 22 μm wide and 40 μm long [12]. Each image is made from 400 different illumination angles. Using an illumination wavelength of 475 nm and a high numerical aperture oil immersion objective (NA = 1.4) a lateral resolution of 97 nm has been achieved, thus demonstrating an experimental value of about λ/(3.5×NA). A further reduction in the illumination wavelength to 405 nm allowed this value to be improved to a resolution of 90 nm [29]. Both of these results clearly show the possibility of imaging below 100 nm in a transmission non-fluorescent microscope. While the axial resolution is not as good, being 300 nm, this can nonetheless be improved to 200 nm by using TDM in the reflection mode [30]. The techniques developed here will find many applications for high resolution, non-invasive imaging of live cells.

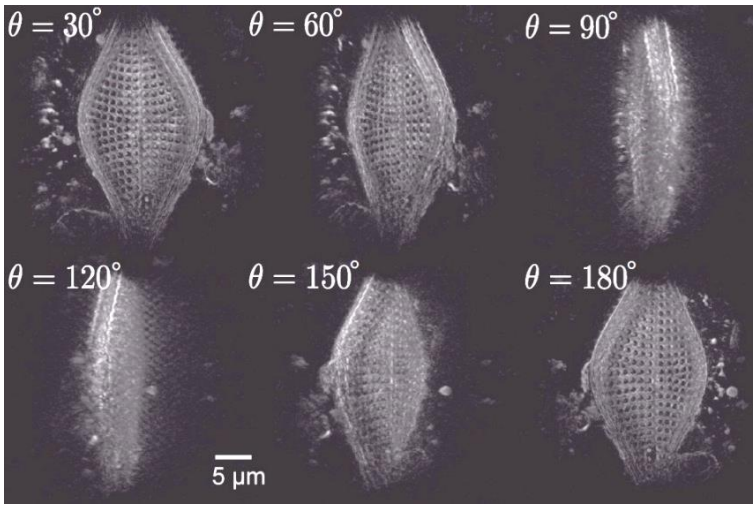

Figure 2. 6 views at different angles of a diatom measured with TDM in the transmission mode, demonstrating a lateral resolution of 97 nm.

2.2. Submerged microsphere optical nanoscopy (SMON)

A second emerging technique for achieving superresolution without labelling is the SMON technique, in which a glass microsphere is placed on the sample, in front of the objective, resulting in a lateral resolution of 50–120 nm in water [13]. Two effects are produced by the glass bead. The first one is the formation of a high intensity subdiffraction limited sized photonic-jet below the microsphere. Photonic nano-jets are better known for their interesting properties ofsuperresolution focusing of laser beams [14] and use in two photon fluorescence enhancement [14, 31] and laser surface nanostructuring [32].By reversing this optical path, superresolution imaging can be achieved.

The second effect is the conversion of the evanescent waves close to the sample into propagating waves that can be collected by the microscope objective to perform far-field imaging. In standard illumination conditions, these waves are very weak but it is the particular focusing properties of the nano-jet by the microsphere that plays an important role in enhancing the signal contrast of the propagating waves outside the microsphere. The resulting image thus contains fine subdiffraction limited detail of the sample that cannot normally be retrieved by classical imaging.

The results illustrated in figure 3(a) show a SMON image of anodic aluminum oxide (AAO) nanopores that are approximately 50 nm in size. A 50x water immersion objective (NA = 0.75) was

used in the transmission modewith a 100 μm microsphere of $BaTiO_3$. A resolution of well below 100 nm is clearly demonstrated. The results in figure 3(b) and (c) are of clusters of 75 nm adenoviruses, shown with SEM in (b) and SMON in (c) using an 80x water immersion objective (NA = 0.9). The samples were prepared by first coating the microscope cover slide with a 5 nm thick layer of gold to enable both optical and SEM imaging. The results show that individual adenoviruses can be identified and thus the superresolution capability of SMON. The TDM and SMON techniques are good illustrations of unlabelled superresolution techniques that are capable of lateral resolutions below the classical limit of 200 nm without using labelling.

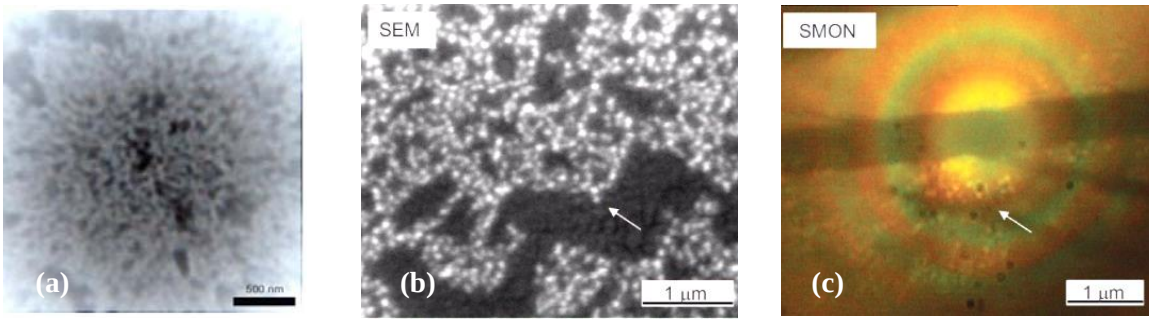

Figure 3. Results of SMON imaging in water with 100 μm $BaTiO_3$ microspheres; (a) SMON image of 50 nm sized AAO nanopores and imaging of clusters of 75 nm adenoviruses by (b) SEM and (c) SMON.

3. Unlabelled nanodetection nanoscopy

As shown in figure 1, the second family of far field nanoscopy techniques concerns those that use nanodetection by which nanostructures are made visible or some parameter connected with them is made observable or measurable without necessarily resolving all the details. This can be achieved without labelling by increasing the contrast, measuring the phase, or using deconvolution techniques. In [7] we described high contrast techniques such as Nomarski and laser scanning tomography (LST) [6] which is more recently known as light sheet microscopy [24, 33]. These different methods are now illustrated with the SEEC technique and strobed phase contrast microscopy for increasing the contrast, high resolution CSI by measuring the phase and TSOM that uses deconvolution techniques.

3.1. High contrast: surface enhanced ellipsometric contrast microscopy (SEEC)

With the size of a nanostructure being well below the Rayleigh limit in a conventional optical microscope, the scattered intensity is so small that it is invisible. The scattered light intensity decreases as a function of d^6 when the object size $d << \lambda$, the well-known phenomenon of Rayleigh scattering.Since scattering is uniform in all directions, by increasing the contrast, nanoparticles can become visible in the far field.

One way of increasing the contrast is to reduce the background signal using an antireflection-coated substrate with polarized light in the SEEC technique [34] in which a 10–100 times improvement in the contrast is achieved. Nanostructures modify the polarization of the reflected light and become visible in a crossed polarized light system. This technique is used with commercially available substrates known as Sarfus® (Nanolane, Le Mans, France) to study carbon and steroid nanotubes, chitin fibres, nanowires and gold nanostructures and dots.

Thin films and nanometrically thin structures extended laterally are often also invisible in classical microscopy due to their very low contrast, even using phase contrast microscopy. The visibility depends on the difference between the refractive index of the structure to be visualized and that of the background, and the extent of the structure laterally across the field. These can become visible with the SEEC technique, such as with lipid layers and vesicles, lectin layers and cell structures. A

successful study has been performed on bacterial motility by observation of just such a thin layer consisting of the slime trails left by the bacteria [15]. This study involved observing the nanometer-thick extracellular matrix (slime) trails left by moving bacteria(delta-proteobacteriumMyxococcusxanthus) in water. Two techniques were used. The first, phase contrast microscopy, was used to show the bacteria themselves (figure 4(a)). Then SEEC was used to show up the slime trails (figure 4(b)). Combining the two images (4(c)) at video rate shows up the movement of the bacteriawithout the need for labelling. This procedure was used to determine the patterns of slime secretion during different velocity phases of the moving bacteria and to analyze the slime-propulsion hypothesis. Such a high-sensitivity technique made it possible to elucidate, for the first time, how slime is deposited during motility and to demonstrate that slime does not mediate propulsion but more likely facilitates motility-driven attachment to the substrate.

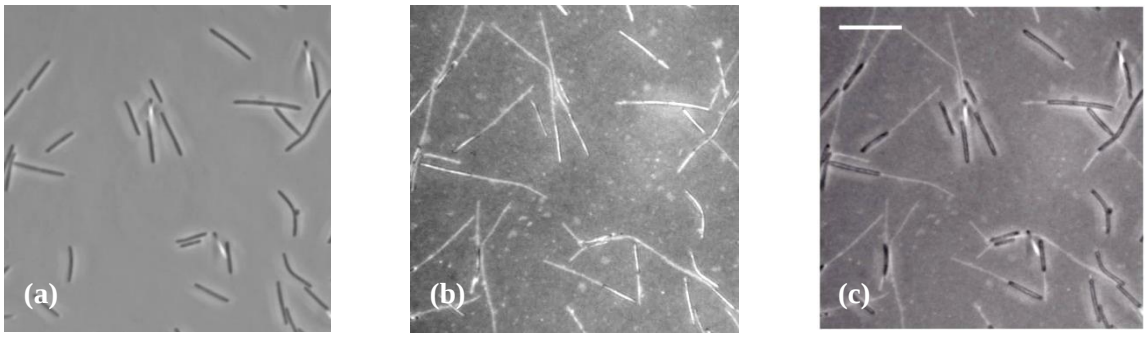

Figure 4. Observation of slime trails in the study of bacterial motility using (a) phase contrast microscopy to show the bacteria, (b) SEEC to reveal the slime trails and (c) phase contrast and SEEC combined to show the bacteria and their slime trails, scale bar: 10 μm (courtesy of Marie-Pierre Valignat, INSERM, Marseille, France).

Other applications concerning the use of SEEC for studying nanolayersare that of graphene, DNA biochips [35], self-organized monolayers of phospholipids[36], enzyme reactions [37]and in specific antibody recognition[38].The advantages of the SEEC technique are the nanometer sensitivity for studying nanolayers and nanoparticles using full field unlabelled imaging in real time and surface roughness and layer thickness measurements by calibrating the z-axis.

3.2. High contrast: strobed phase-contrast microscopy

While the previously mentioned slime trails were not visible with phase contrast microscopy, given the right conditions, even imaging atomic-sized structures becomes possible, such as dislocations in semiconductor crystals when extended in one of the imaging dimensions and associated with a sufficient variation in refractive index of the strain field[39].

The study of the properties of 5 nm thick unilamellarlipid membranes in the form of giant vesicles is important to help understand complex cell functions, the role of vesicle formation and transport, and the development of synthetic cells.While not directly visible perpendicularly to the membrane, the edges of such vesicles do becomevisible in phase-contrast microscopy, with the refractive index being about 10% higher than that of the aqueous surroundings. The dynamic thermal shape fluctuations of giant vesicles (10 μm radius, figure 4(a)) have been studied using strobed phase contrast microscopyto reduce the measurement uncertainties of the bending elasticity of lipid membranes [40]. Since thermal fluctuations are very complex, resulting from the addition of many different vibration modes, the higher frequency movements become blurred during the acquisition time of a single standard video image (40 ms). Stroboscopic illumination with a xenon flashlamp to freeze this movement reduces the blurring, as illustrated by the single sample image in figure 4(a). The positions of the membraneare measured from the minimaof the intensity profiles through the centre of the near circular vesicle. The

time dependent fluctuations are measured from repeated measurements acquired at frame rate (25 images per second) to obtain a long image sequence (10^4 images).

A further improvement in the measurements of the bending modulus to reduce the uncertainty resulting from various artifacts (vesicles with defects) has been achieved using more sophisticated measurement procedures. Selection criteria are used on the series of images of moving vesicles to retain only certain images that satisfy the requirements of the applied theory [16]. These criteria are defined from certain parameters to test four quadrant arc shapes within the region of interest (ROI) that represents a ring containing the vesicular contour delimited by two concentric circumferences with internal radius R_{int} and external radius R_{ext} ($R_{int}<R_{ves}<R_{ext}$). These delimit the contour, where R_{ves} is the vesicle radius, (figure 4(b)).This procedure has been successfully used to measure the bending moments of 1-stearoyl-2-oleoyl-sn-glycero-3-phosphocholine lipid membranes, as well as to estimate the friction between the monolayers making up the bilayer.

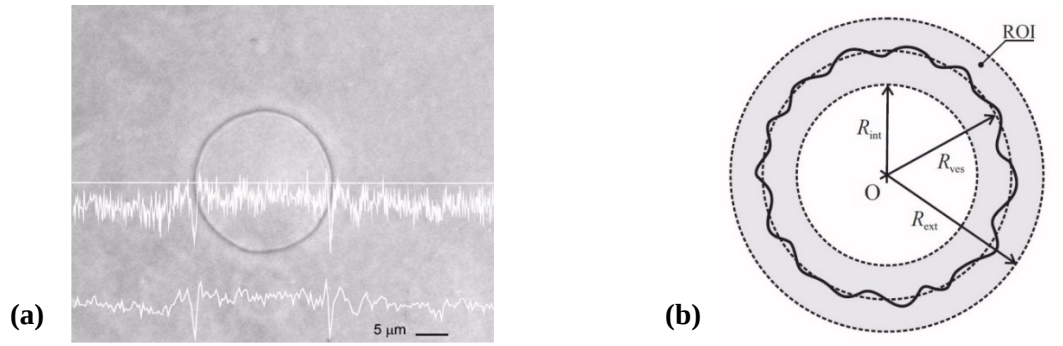

Figure 4. Measurement of dynamic thermal shape fluctuations of a giant vesicle using strobed phase contrast microscopywith (a) a single sample image of a vesicular contour with intensity profiles before (upper) and after processing (lower) and (b) a region of interest (ROI) containing the vesicular contour used to define selection criteria of the measured vesicles (courtesy of J. Genova et al. [16, 40], Laboratory of Liquid Crystals, ISSP, BAS, Sofia, Bulgaria).

3.3. Phase measurement: high resolution coherence scanning interferometry (CSI)

Information from nanostructures can also be obtained by measuring the phase of the light in interference microscopy. CSIis commonly used for measuring nanometric surface roughness (along the optical axis) of materials using quantified interferometry in an optical microscope equipped with specific interference objectives [41].

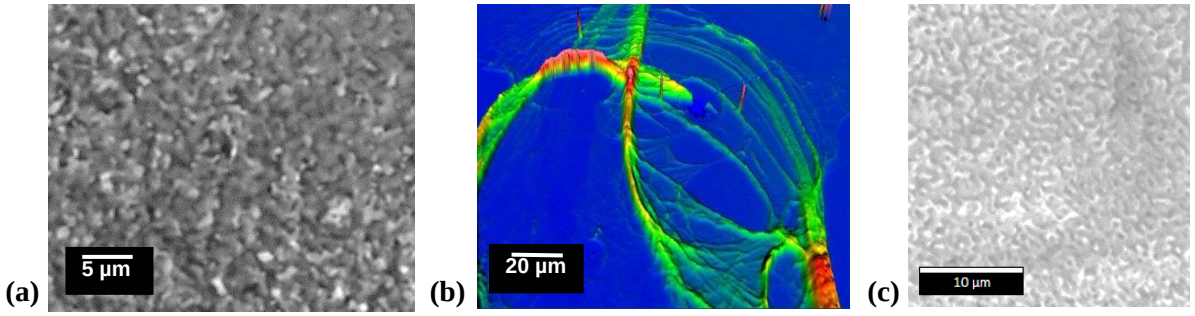

Figure 5. Nano surface roughness measurements using CSI of(a) PPHMDS layer dipped in Fibronectin withR_t = 1.57 µm (Leitz-Linnik), (b) fibres of fibronectin (R_t = 30 – 300 nm) on PPHMDS layer used for new biomaterials (ZygoNewView 7200) and (c) self-organized circular nano ripple structures on stainless steel with period = 1 µm and R_t = 600 nm (Leitz-Linnik) [19]

The results in figure 5(a) and (b) show some different measurements of a PPHMDS (polymerized hexamethyldisiloxane) layer dipped in fibronectin, both commonly used in biomaterials development. The local fine roughness of the layer is given in figure 5(a) and the fibre structures shown in figure 5(b) [18]. A second application example is given in figure 5(c) of self-organizednanostructured "ripples" made on stainless steel with a fs pulsed IR laser (λ = 1030 nm, 300 fs pulses). The results show circular nano ripples made using circularly polarized light, with nanostructures having a period of 1 µm, and a total roughness (peak-valley roughness) of R_t = 600 nm [23]. Variations in the laser parameters allow the modification of the colour aspect and wetting behavior of the surface. The technique has been further developed for real time measurement using a high speed camera and FPGA processing to achieve a 3D image acquisition rate of over 20 images per second [42].

CSI can also be used for imaging interfaces and structures buried under transparent layers but in this case, the signal to noise ratio can be very poor due to low reflectivity, noise and artefacts [43]. The depth profile images in tomographic analysis, also known as full-field OCT [44]can also be degraded so much that structures near to the Rayleigh limit in size are lost in the noise [45]. By means of a series of noise reduction techniques, in [20] we demonstrated how much finer details can be observed of small pores buried in a Mylar polymer film of 3.6 µm thickness. This material is important for use as an insulator in electronics and micro-electronics. The system used is an adapted Leitz-Linnik interference microscope with x50 objectives (NA = 0.85) and a CCD camera. By using image averaging to reduce temporal noise, subtraction of the "dark" image to reduce the fixed pattern noise of the camera and division by the "flat field" image of a white test target to reduce image defects from dust on the optical components, much higher quality tomographic profile images are obtained.

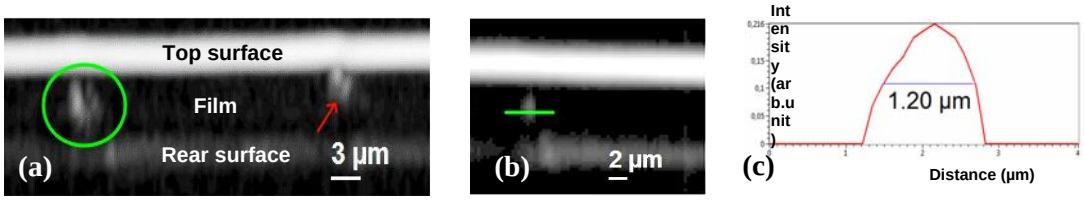

Figure 6. Improved defect analysis in a 3.6 µm thick Mylar film using high resolution tomographic CSI showing (a) depth profile (XZ) image after 10x averaging showing improved details of defects (circle and arrow) previously buried in noise,(b) depth profile (XZ) image after 100x averaging and dark and flat correctionsand (c) improved profile of small pore from line in (b)[20]

The results given in figure 6(a) show the improvement after averaging 10 images and in (b) after 100 images together with dark and flat corrections (in a different place from (a))[20]. In this way, near-diffraction limited sized structures initially lost in noise can be observed (figure 6(c)).

3.4. Deconvolution techniques:Through-focus Scanning Optical microscopy (TSOM)

The third method of nanodetection consists of using deconvolution techniques, applicable more in the case of regular small structures. For example, TSOM is a new method that uses an ordinary optical reflection microscope at visible wavelengths to give subnanometer dimensional sensitivity in the critical dimension measurement of nanostructures in micro-electronics[21].

By scanning through the focus of the microscope and sampling the XY images as a function of Z, the observation of the XZ image near to the focus reveals a large amount of information concerning the size of nanostructures, with sub-nm sensitivity. Great care is paid in optimizing the image acquisition conditions (averaging, noise reduction, calibration…) and in normalizing the images so that they can be compared between each other or with a library of images from calibrated standards.

The results in figure 7(a) show a typical result of a differential TSOM image of 40-50 nm wide lines in Tri-gate FinFETtransistors (Intel). A comparison of the intensity profiles (averaged over 8 lines) illustrates the difference (green profile) between a 44.2 nm wide line (blue profile) and a 55.3 nm wide line (red profile), that have a uniform height of 71.4 nm. The images were made at a wavelength of λ = 546 nm and an imaging objective with NA = 0.8. Although the optical lateral

resolution limit is only 0.42 μm, the cross section of the diffraction pattern of the 40 nm wide line is observable because of the high contrast provided by the optimized imaging and acquisition.The results in figure 7(b) show finite difference time domain (FDTD) simulations to predict how TSOM would perform for measuring structural perturbations for 22 nm and 16 nm node transistor fins. The results show that TSOM would have sufficient sensitivity to several critical parameters such as fin width, sidewall angle (SWA), fin height, high-k (dielectric constant) material layer thickness, BOX (buried oxide) recess, and pitch walk (aperiodicity of fin walls). The TSOM technique can also be used for measuring the size of nanoparticles as small as 20 nm in diameter and to determine the number of particles in clumps of 1 to 4 nanoparticles of 120 nm in size.

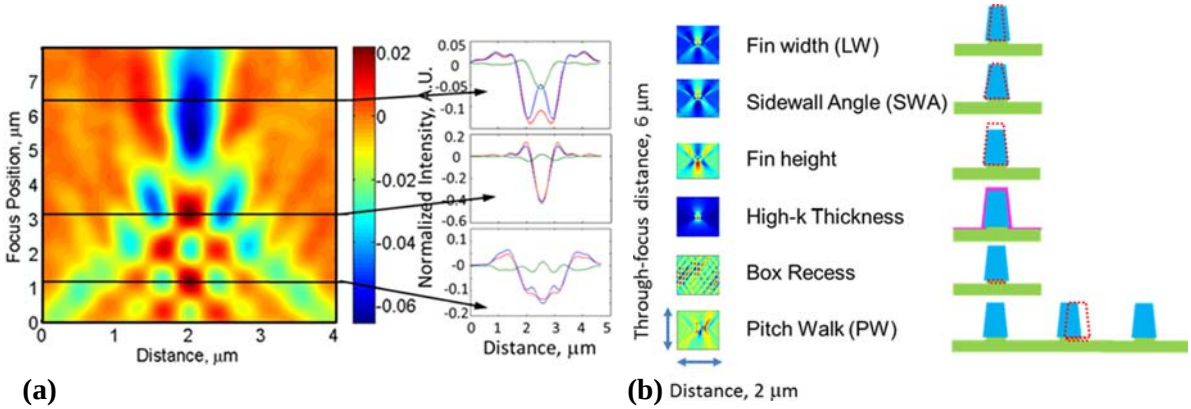

Figure 7. Results of critical dimension measurement of nanometricfins in microelectronics using TSOM;(a) difference in measurements using differential TSOM (green profile) between 44.2 nm wide line (blue profile) and 55.3 nm wide line (red profile) and (b) simulation images for differential TSOM (left) for different parameter perturbations of sub-22 nm node lines (right).

4. Conclusions

In this review we have presented an improved classification scheme of the many optical nanoscopy techniques that exist and in particular underlined the emerging far field superresolution and nanodetection techniques that do not require labelling. Superresolutionhas been illustrated with TDMshowing a resolution of 97 nm on 3D views of diatoms and SMON for imaging viruses of less than 100 nm in size. Nanodetection techniques using contrast improvement have been illustrated with the SEEC technique for real time imaging of bacteria motility and strobed phase contrast for improved measurement of the bending moments of lipid membranes as well as to estimate the friction between the monolayers making up the bilayer. The use of phase measurement using interference microscopy in high resolution tomographic imaging has been improved using image acquisition/processing of μm pores in Mylar polymers. Finally, deconvolution techniques have been shown using TSOM and the careful control and calibration of intensity profiles for critical dimension measurement in nanostructures for microelectronics.

We thus demonstrate that there are a growing number of far field optical nanoscopy techniques that do not require labelling but that are capable of resolving nanostructures below 100 nm in size or providing useful information of nanostructures down to nm and sub-nm measurement sensitivity.

Acknowledgments

Thanks are extended to P. Pfeiffer for the measurements on the fibronectin.

References

[1] Ehrenberg M 2014 The Royal Swedish Academy of Sciences, Stockholm, Sweden
[2] Klar T A, Jakobs S, Dyba M, Egner A and Hell SW 2000 *Proc. Natl. Acad. Sci. USA* **97**8 206

[3] Dickson RM, Cubitt A B, Tsien RY and Moerner W E 1997 *Nature* **388** 355
[4] Betzig E, Patterson GH, Sougrat R, Wolf Lindwasser O, Olenych S, Bonifacino J S, Davidson M W, Lippincott-Schwartz J and Hess H F 2006 *Science* **313** 1642
[5] Montgomery P C 1990 *Nanotechnology* **1** 54
[6] Fillard JP 1996 *Near Field Optics and Nanoscopy* (Singapore: World Scientific)
[7] Montgomery PC, Montaner D, Anstotz F and Serio B 2012 *J. Phys. Conf. Ser.* **398** 012001
[8] Montgomery P C and Leong-Hoi A 2015 *J. Nanotech., Sci. Appl.* **8** 31
[9] Bretschneider S, Eggeling C and Hell SW 2007 *Phys. Rev. Lett.* **98** 218103
[10] Gustafsson MG. 2005 *Proc Natl Acad Sci U S A* **02** 13081
[11] Montgomery PC, Serio B, Anstotz F and Montaner D 2013 *Appl. Surf. Sci.* **281** 89
[12] Debailleul M, Georges V, Simon B, Morin R and Haeberlé O 2009 *Opt. Lett.* **34** 79
[13] Li L, Guo W, Yan Y, Lee S, and Wang T 2013 *Light: Sci. & Appl.* **2** e104
[14] Lecler S, Takakura Y and Meyrueis P 2005 *Opt. Lett.* **30** 2641
[15] Ducret A, Valignat MP, Mouhamar F, Mignot T and Theodoly O 2012 *Proc. Natl. Acad. Sci. USA* **109** 10036
[16] Genova J, Vitkova V and Bivas I 2013 *Phys.Rev. E Stat Nonlin Soft Matter Phys.* **88** 022707
[17] Pecheva E, Montgomery P, Montaner D and Pramatarova L 2007 *Langmuir* **23** 3912
[18] Pramatarova L, Radeva E, Pecheva EHikov T, Krasteva N, Dimitrova R, Spassov T, Mitev D, Montgomery P and Sammons R 2011 *On Biomimetics*, Ed. Pramatarova L (InTech) **14** pp 297-320
[19] Hairaye C, Mermet F, Engel T, Montgomery PC and Fontaine J 2014 *J. Phys.Conf. Ser.* **558** 012063
[20] Leong-Hoi A, Claveau R, Flury M, Uhring W, and Montgomery P 2015 *Proc. SPIE* **9528** 952807
[21] Attota R, Bunday B and Vartanian V2013 *Appl. Phys. Lett.* **102** 222107
[22] Born M and Wolf E 1980 *Principles of Optics: Electromagnetic Theory of Propagation, Interference and Diffraction of Light* 6th ed. (Oxford: Pergamon Press)
[23] Mashanov GI, Tacon D, Knight AE, Peckham M and Molloy J E 2003 *Nat. Methods* **29** 142
[24] Mahou P, Vermot J, Beaurepaire E, Supatto W 2014 *Nat.Methods* **11** 600
[25] Bewersdorf J, Schmidt R and Hell SW2006 *J. Microscopy* **222** 105
[26] Van Putten E, Akbulut D, Bertolotti J, Vos W, Lagendijk A and Mosk A 2011 *Phys. Rev. Lett.* **106** 193905
[27] Choi Y, Kim M, Yoon C, Yang T D, Lee K J and Choi W 2011 *Opt. Lett.* **36** 4263
[28] Liu Z, Lee H, Xiong Y, Sun C and Zhang X 2007 *Science* **315** 1686
[29] Cotte Y, Toy F, Jourdain P, Pavillon N, Boss D, Magistretti P, Marquet P and Depeursinge C 2013 *Nat. Photonics* **7** 113
[30] Liu H, Bailleul J, Simon B, Debailleul M, Colicchio B, Haeberlé O 2014 *Appl. Opt.* **53** 748
[31] Lecler S, Haacke S, Lecong N, Crégut O, Rehspringer J and Hirlimann C 2007 *Opt. Expr.* **15** 4935
[32] Guo W, Wang ZB, Li L, Liu Z and Luk'yanchuk B 2008 *Nanotechnology* **19** 455302
[33] Ritter JG, Veith R, Veenendaal A, Siebrasse JP and Kubitscheck U 2010 *PLoS One* **5** 11639
[34] Ausserré D and Valignat M P 2007 *Opt.Expr.* **15** 8329
[35] Monot J, Petit M, Lane SM, Guisle I, Léger J, Tellier C, Talham D R and Bujoli B 2008 *J. Am. Chem. Soc.* **130** 6243
[36] Gunnarsson A, Bally M, Jönsson P, Médard N and Höök F 2012 *Anal. Chem.* **84** 6538
[37] Egea AMC, Metivier M, Croguennoc P, Remaud-Simeon M and Vieu C 2013 *BioNanoScience* **4** 37
[38] Souplet V, Desmet R and Melnyk O 2007 *J. Pept. Sci.* **13** 451
[39] Montgomery PC and Fillard JP 1989 *Electron. Lett.* **25** 89
[40] Genova J, Zheliaskova A, Vitkova V and Mitov MD 2009 *J. Optoelectron. Adv. Mater.* **11** 1222
[41] Schmit J, Reed J, Novak E and Gimzewski JK 2008 *J. Opt. Pure Appl. Opt.* **10**(6) 064001

[42] Montgomery P, Anstotz, F, Johnson G and Kiefer R 2008 *J. Mater. Sci. Mater. Electron.* **19** 194
[43] Benatmane A and Montgomery PC 2004 *Eur. Phys. J. Appl. Phys.* **27** 411
[44] Dubois A, Grieve K, Moneron G, Lecaque R, Vabre L and Boccara AC 2004 *Appl. Opt.* **43** 2874
[45] Montgomery P C, Montaner D and Salzenstein F 2012 *Proc. SPIE* **8430** 843014